Journal of
Experimental and Theoretical Analyses

MDPI

Article

Preliminary Numerical Modelling of the Ionization Region to Model Ionic Propulsion

Jason Knight [1,*], Mojtaba Ghodsi [1], Bradley Horne [2], Edward John Taylor [3], Niah Laurel Virhuez Montaño [1], Daniel George Chattock [1], James Buick [1], Ethan Krauss [4] and Andrew Lewis [5]

[1] School of Electrical and Mechanical Engineering, University of Portsmouth, Anglesea Building, Anglesea Road, Portsmouth PO1 3DJ, UK; up918467@myport.ac.uk (N.L.V.M.); up2008004@myport.ac.uk (D.G.C.)
[2] Veolia Nuclear Solutions, 18 Nuffield Way, Abingdon OX14 1RL, UK
[3] Renishaw, New Mills, Wotton-Under-Edge GL12 8JR, UK; up906032@myport.ac.uk
[4] Electron Air LLC, 52 Union St, Oberlin, OH 44074, USA
[5] School of Physics, Engineering & Computer Science, University of Hertfordshire, College Lane, Hatfield AL10 9AB, UK; a.lewis@herts.ac.uk
* Correspondence: jason.knight@port.ac.uk

Abstract

Ionic propulsion, where charged particles, ions, are produced between electrodes and accelerate towards the negative electrode, has practical applications as a propulsion system in the space industry; however, its adoption to in-atmosphere ionic propulsion is relatively new and faces different challenges. A high potential difference is required to achieve a corona discharge between a positive and negative electrode. In this work, we will explore the feasibility of ionic propulsion using CFD modelling to replicate the effect of the ions, with a future aim of improving efficiency. The ionization region is modelled for a 15 kV potential difference, which is replicated with a velocity inlet, based on experimental data. The output velocity from the numerical simulation shows the same trend as theoretical predictions but significantly underestimates the magnitude of the ionic wind when compared with theoretical estimates. Further modelling is highlighted to improve predictions and assess if the theoretical model overestimates the ionic wind.

Keywords: ionic wind; corona discharge; sustainable aviation; electro-aerodynamic devices; thrust

Academic Editor: Marco Rossi

Received: 18 August 2025
Revised: 11 November 2025
Accepted: 24 November 2025
Published: 11 December 2025

Citation: Knight, J.; Ghodsi, M.; Horne, B.; Taylor, E.J.; Virhuez Montaño, N.L.; Chattock, D.G.; Buick, J.; Krauss, E.; Lewis, A. Preliminary Numerical Modelling of the Ionization Region to Model Ionic Propulsion. *J. Exp. Theor. Anal.* **2025**, *3*, 42. https://doi.org/10.3390/jeta3040042

1. Introduction

The basic principle behind ionic propulsion arises from the use of two electrodes with a potential difference between them. When the potential difference is sufficiently high, electrons will flow between the electrodes. These electrons will collide with neutral atoms, producing an ionic wind and a corresponding force, or thrust, in the opposite direction to the flow of the electrons. Harnessing this thrust to power an aircraft would provide the double advantage of a potentially carbon-neutral power source for sustainable aviation and a quiet propulsion system reducing noise pollution for passengers and in the regions surrounding airports. Ionic propulsion has attracted increased research interest in recent years, and the key developments are highlighted in the rest of this section.

An aircraft powered by ions would be quiet and potentially carbon neutral, and have a lower failure rate than those powered by conventional engines due to the absence of moving parts within the engine. The basis of ionic propulsion is to have two electrodes, one negative and one positive. As the potential difference between the electrodes increases,

electrons will start to flow between the electrodes. As the electrons pass through space, they collide with neutral atoms in the atmosphere. This creates an ionic wind, which creates a force in the opposite direction of the flow of electrons. This force is thrust, which could potentially be used to power sustainable aircraft.

The origin of ionic wind stems from the corona discharge that was found in 1672 by Otto Von Guericke [1]. Von Guericke created a sulfur globe model, in which he performed multiple electrical experiments. Rubbing the surface of the device was found to produce static electricity as the electrical charge accumulated. In 1750, a device known as 'The Electric Fly' was invented [2]. The device consisted of a thin brass or iron wire that had sharp ends and was formed into an S-shape. The wire was supported at its midpoint by a metal holder and allowed to rotate. The other end of the holder was fixed onto a piece of wood. Once an electric charge is delivered to the wire through the holder, the wire begins to rotate like a pinwheel. Using a similar principle in 1929, Thomas Townsend Brown built a device that uses ionic wind to generate movement [3].

These devices are now known as Electro-Aerodynamic Devices (EADs) that generate propulsion without any moving parts in neutral fluid regions [4–7]. EADs use electricity to create an electromagnetic field between an anode and a cathode. In the electro-magnetic field, negatively charged ions are produced and repelled by the electrostatic force of the positively charged anode towards the negatively charged cathode. As they are repelled, the ions collide with neutral particles in the fluid (air). The collisions induce a propulsive force, thus creating ionic wind [8]. EADs use this ionic wind to fly. The wind can be directed vertically to oppose weight or directed horizontally to pass over wings, producing lift.

In contrast to conventional propulsion systems such as propellers, rotors, or jet engines, ionic propulsion produces no pollution and very little noise. Another benefit is that there are no moving parts, meaning that less maintenance is required. However, although there are many benefits to using ionic propulsion, the main drawback is that it is difficult to produce a device that can use ionic propulsion to a scale that is suitable for transportation.

Until recently, EADs have not been able to fly with their power source onboard. This is primarily due to the weight of the components needed to produce the high voltages required [9]. To get around this, several lightweight power converters were required for EADs. The first EAD with an onboard power supply was created by Ethan Krauss, Electron Air LLC [10], which was patented for lifting its power supply against Earth's gravity using ion propulsion [4,11]. The VTOL design requires a geometry optimized for efficiency and a miniaturized electrical system. In 2018, the Massachusetts Institute of Technology (MIT) used the same technology in the horizontal plane to power a model with a 5 m wingspan. Their design converted the battery voltage of −225 V battery to 40 kV output and provided up to 565 W of power with an efficiency of 85% and a specific power of 1.15 $kWkg^{-1}$ [12]. The craft flew a total of 60 m (the team was limited to the size of the sports hall they used for testing). The team's final design resembled a large, lightweight glider with a 5-m wingspan and weighed approximately 2.27 kg, with most of the weight coming from the batteries. The rudder and elevator surfaces were actuated with electronic servos, which were trimmed for straight flight, but adjusted during flight by the pilot via remote radio control during launch and landing. Other than this, the craft had no other moving parts. The craft was powered by a stack of lithium–polymer batteries, which fitted within the fuselage. The batteries produced 40 kV to support the sustained flight [5]. Although the craft did manage sustained flight, the team had to use a launching runway fitted with an elastic cable system that provided enough force to accelerate the craft from a standstill and get it airborne. Once in the air, the ion engines provided enough energy to sustain the flight. However, the ionic propulsion method still had a much lower efficiency than conventional propulsion. Another area of study in aeronautical applications is the use of

EAD flow to aid in the control of boundary-layer airflow near the surface of an airfoil using plasma actuators [6]. This technology would reduce turbulence near the surface, improving efficiency and, thus, increasing the fuel economy and speed of the aircraft.

The use of EAD technology could be utilized for several practical applications away from its use in in-atmosphere aircraft. One application is cooling, which is an active area of study [13]. As computing performance increases and the size of devices decreases, the amount of heat emitted from the components also increases [14]. In the use of microelectronics, an EAD device could be created where the ionic flow between two electrodes could be used to pass over hot components, supplying cooler air towards the components and drawing the hot air away, removing the use of a traditional fan-based system. Another area is the use of corona discharge in water, which could be used in the treatment of drinking water and wastewater [15]. By establishing an electric field in a water stream, chemical and physical reactions are created. These include small shockwaves, bubbles, and a limited amount of UV radiation. This leads to the elimination of bacteria and viruses in the water and the removal of dirt build-up in supply pipelines.

2. Influential Factors for Ionic Wind Calculations

There are multiple factors that may affect the thrust produced during ionic propulsion. These factors need to be understood to maximize the thrust and to produce the ideal conditions for flying, for example, the distance between the anode and the cathode, more commonly referred to as the electrode spacing. Bouazza et al. [16] have predicted the flow of ions and the force they carry once they leave the wire. The further the ions travel from the wire during corona discharge, the weaker the force produced. Therefore, if the distance between the electrodes is too large, the ionic wind induced will be much weaker. This claim is backed up by experimental data [4], where it is evident to see that the distance between the electrodes has a direct effect on the amount of voltage needed to create thrust. Xu et al. [4] found that when using an electrode spacing of 50 mm to generate 50 mN/m of thrust, a voltage of 29 kV is required, whereas with a spacing of 300 mm, a voltage of 62 kV is needed, which is 2.1 times the amount of voltage needed with a 50 mm spacing. However, Xu et al. [4] also showed that larger gap spacings can have higher thrust-to-power ratios. For instance, increasing the gap spacing from 50 mm to 200 or 300 mm could increase the thrust-to-power ratio up to two- or three-fold. Although bringing the emitter wires closer to the collector surface generated more thrust, it also caused a steep increase in current draw, leading to greater joule heating and, consequently, higher power losses [6]. Therefore, electrode spacing must be considered when designing an EAD, as the larger the spacings between electrodes, the weaker the electro-magnetic field and ionic wind, but potentially higher efficiencies can be achieved.

The higher the voltage, the larger the thrust, thus increasing the amount of ionic wind produced, as found by Chirita and Ieta [17]. However, at atmospheric pressure, the breakdown voltage in air is ~3 kV/mm [18]. This implies that at lower distances, the voltage applied would have to be limited to prevent an electric arc from forming between the electrodes, thus reducing the amount of thrust produced by the proposed EAD design. Hence, a compromise is needed.

The size in diameter and length of the emitter wire, and the collector size and shape are also important considerations. The emitter wire's cross diameter should be as small as possible to improve ionization, but large enough to withstand mechanical and thermal damage. The length of the emitter wire should be long enough to generate adequate thrust, whilst not too short, which could cause overheating of both the power supplies and the wires themselves [6]. The collector diameter is the distance across the cross-section of the collector. The collector diameter directly affects the thrust produced during ionic propulsion.

With a larger area, the attractive force is increased due to the greater surface area attracting ions, meaning more ions are pulled by the electrode, thus inducing a stronger wind. A collector diameter of 10 mm will produce about 145 mN/mm of thrust at 80 kV [4], whereas a collector diameter of 38 mm produces a thrust of 200 mN/mm. This is a 37.9% increase in thrust for a diameter that is 280% larger. The use of multi-stages can produce more thrust per area, but multi-stages exhibit diminishing returns with each additional stage due to reduced efficiency. Using a larger diameter for an airfoil that is to experience ionic wind or using multi-stages will increase the overall mass, meaning more force is needed, which would need, in turn, either a higher voltage or an even larger collector diameter, which in turn further increases the mass of the plane. For this reason, the collector diameter and use of multi-stages need to be taken into careful consideration when designing an EAD [6].

Another important factor to consider is the temperature. The temperature can have a drastic effect on ionic propulsion. At high temperatures, particles gain more kinetic energy, which in theory, is beneficial, as the higher the kinetic energy, the more collisions occur, and the more energy is transferred during those collisions, resulting in a higher propulsive force. This is supported by previous studies that show that as the temperature rises, the current density rises along with it. Current density is termed the ion current through a unit area [19]. With more ions travelling through a particular area due to the increased kinetic energy—in this case, between the electrodes—more collisions can occur, thus making the air between the electrodes highly conductive. The results from a study show that at 373 K, the current density is 0.007 mA/m, while at 973 K, the current density is 0.87 mA/m [20]. These results reveal that at 973 K, an EAD will produce more thrust. Although the temperatures in the experiment are very high, this information is vital, as it confirms the theory. When the relative humidity is increased, the ionic wind velocity decreases [21]. The current was also measured against the relative humidity, which shows it decreasing as the relative humidity increases. Therefore, the overall effect on the ionic propulsion is that it decreases as the overall thrust is reduced. Lee and Lau [22] also show that there is a relation between how positive and negative ionic winds affect the current readings based on a change in relative humidity.

3. Theoretical Calculations for In-Atmosphere Ionic Propulsion

The theoretical equations in this section have been taken from the literature [23–25] and are included here to aid clarity of the subsequent theoretical predictions presented later. A more detailed explanation of most of the formula in this section can be found in Perkins and Thompson [23]. During corona discharge, positively charged ions travel from the emitter to the receiver. During this journey, they collide with air particles, which accelerate towards the collector, producing thrust, as shown in Figure 1.

Figure 1 shows how ions travel and collide with neutral air molecules between the electrodes and transfer momentum before re-accelerating towards the opposite electrode to create ionic wind. The region of the air current produced by this process is called the ionic region and is directly proportional to the area of the emitter [23]. It can be found using the following formula:

$$\delta = \sqrt{a} \tag{1}$$

where a is the radius of wire or tip radius of a point, and δ is the thickness of the ionization region. The thrust produced by the ionic thruster is proportional to the distance between the two electrodes and the current in the discharge. It is found that if the voltage is increased too much between the electrodes, the medium (in this case air) between the electrodes will break down, causing a spark. This must be avoided, as it is the glow breakdown that is required for ionic propulsion, which occurs before sparking. The ion mobility affects this breakdown and will be different depending on the atmospheric conditions. Christenson

and Moller [24] derived the formula whereby the thrust in Newtons generated, T, by the ionic wind in air is as follows:

$$T = Id/\mu \tag{2}$$

where I is the current in the discharge (amps), μ is the ion mobility ($m^2/V.s$), and d is the gap between electrodes (m). The power generated by the ionization zone is equivalent to the amount computed for the thrust. The thrust per unit power may therefore be determined using the following formulae:

$$P = IV \tag{3}$$

$$\theta = T/IV \tag{4}$$

$$\theta = (d/V)/\mu \tag{5}$$

$$\theta = 1/E\mu \tag{6}$$

where θ is the thrust per unit power (N/kW); V is the applied voltage (V); and $E = V/d$, which is the average electric field (V/m). The efficiency of the ionic thruster will be determined by how much thrust can be created per unit of power into the thruster, which is what must be optimized.

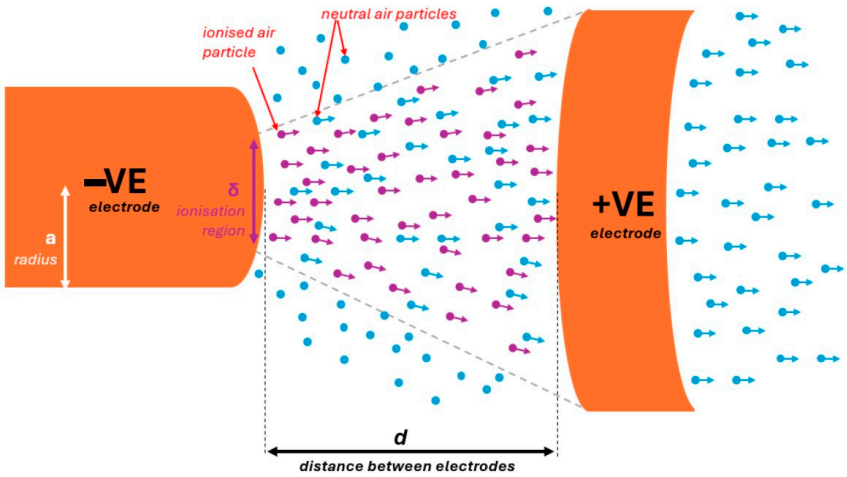

Figure 1. Diagram shows ion collisions and momentum transfer to neutral air molecules.

Equation (2) may be derived assuming that a voltage of V (volts) is supplied and that the electric field is uniform in the main area of the corona discharge. Since no more ions can be produced once the ions have left the high field area surrounding the tip, the product of the discharge cross-section, A, and the ion density, μ, will stay constant. T_i, the electrostatic force experienced by each ion, is formulated as follows:

$$T_i = eE \tag{7}$$

where e is the unit of charge, and, naturally, the forces acting on the electrodes are equal and opposing. The total force of all the ions on the electrodes is as follows:

$$T = NT_i = NeE \tag{8}$$

where N, the total number of ions in the discharge, is $N = n_i Ad$. The discharge current is given by the following:

$$I = n_i e v_i A \tag{9}$$

where A is the discharge cross-section; n_i is the product of ion density; and v_i is the average ion velocity, which is given by $v_i = \mu E$. Thus, the total force acting on the electrodes is as follows:

$$T = NeE = n_i AdeE = n_i e v_i AdE/\mu E = Id/\mu \quad (10)$$

Since the ions are assumed to be in a homogeneous field, their acceleration will be constant, a, which is determined by the following:

$$a = eE/m_i \quad (11)$$

where m_i is the mass of the ion. On average, an air molecule will collide with the ion after a distance from the emitter, λ—the mean free path of the ions in air. If it is assumed that the ion transfers all its momentum to the ion during the collision, then the ion will be brought to rest during the collision. The ion will have therefore travelled distance λ in each time, t, as follows:

$$\lambda = at^2/2 \quad (12)$$

Thus, the average velocity of the ion leaving the emitter is as follows:

$$v_i = \lambda/t = at/2 = (eE/2m_i)(2m_i\lambda/eE)^{1/2} = E(e\lambda/2m_iE)^{1/2} \quad (13)$$

Depending on the air saturation, the ion mobility of air can vary. The ion mobility of air is known to be 2.14×10^{-4} $m^2/V{\cdot}s$ for dry air and 1.6×10^{-4} $m^2/V{\cdot}s$ for saturated air [26]. It is also possible to compute the ion mobility value as v_i/E; thus, the ion mobility, μ, can be formulated using the following:

$$\mu = (e\lambda/2mE)^{1/2} \quad (14)$$

where μ is the ion mobility ($m^2/V{\cdot}s$), λ is the distance travelled by the ion (m), m is the mass of the ion, and E is the average electric field strength.

The conclusion that ion mobility is proportional to the inverse square root of the electric field is consistent with findings reported for ions in air at high electric fields [25]. When an ion travels the distance (d) between the emitter and collector, it will collide d/λ times. This is due to the ion still being in the electric field (between the emitter and receiver), and so, after each collision, it will therefore accelerate again. The air molecule receives momentum from the colliding ions, given by $2m_iv_i$. This supposes that equal-mass ions and air molecules collide head-on. Consequently, the magnitude of the force accelerating the air, F, or the total momentum imparted to it each second, is as follows:

$$F = 2nm_iv_id/\lambda \quad (15)$$

where n is the number of ions arriving at the collector per second = I/e. Inserting this and Equation (13) for v_i into Equation (14), the force accelerating the air is as follows:

$$F = Id(2m_iE/e\lambda)^{1/2} \quad (16)$$

Using Equation (16) to rewrite the formula as

$$F = Id/\mu \quad (17)$$

it is evident from this that the force that accelerates the air, or the momentum imparted to the ionic wind, is the same as the thrust applied to the electrodes that is a response to the electrostatic force acting on the ions.

The ionic field is generated throughout the entire area of the ionization region, B. Greater thrust and ionic wind production result from more particles gaining a positive charge across bigger areas. If the emitter is a wire or needle tip, the area it produces will have a constant thickness, as determined before, creating a circular zone for ionization. Thus, the area may be computed as follows:

$$B = \pi(\delta/2)(L/4) \tag{18}$$

where L is the length of the wire to the number of emitter points; B is the total area of the ionization region (m^2); and δ is the thickness of the ionization region, and it takes the place of the circular area's diameter. Using the above equation to find ionic wind velocity, it can be calculated as follows:

$$v = T/B\rho \tag{19}$$

where v is the ionic wind velocity (m/s), and ρ is the density of fluid. The density for air at sea level is given as 1.225 kg/m^3 at 15 °C. Air from the ionic zone flows towards the collector at a velocity known as the ionic wind velocity. The negatively charged collector draws the flow towards it. A more detailed explanation of most of the formulae above can be found in Perkins and Thompson [23].

4. CFD Simulation of Ionic Wind

The modelling software Star CCM+ 12 was chosen, as it can simulate both electromagnetic and physical-fluid flow phenomena. The coupling between fluid flow and electrical potential is handled through a multiphysics framework in STAR-CCM+ 12 that allows for a simultaneous solution of fluid dynamics and electromagnetics. STAR-CCM+ 12 uses the Navier–Stokes equations and continuity equation for fluid flow, and they are solved using the finite volume method (FVM). Electromagnetic phenomena are modelled using Maxwell's equations, which govern electric and magnetic fields, and are also solved using FVM. The electric field, **E**, is derived from the electric potential, ϕ:

$$\mathbf{E} = -\nabla\phi \tag{20}$$

STAR-CCM+ solves Poisson's equation for ϕ:

$$\nabla.(\varepsilon\nabla\phi) = -\rho_e \tag{21}$$

where ε is the permittivity of the fluid, and ρ_e is the free charge density. The electric field contributes a body force, $\mathbf{F}_e$, in the momentum equation:

$$\mathbf{F}_e = \rho_e\mathbf{E} \tag{22}$$

This force is added as a source term in the Navier–Stokes equations:

$$\rho(\mathbf{u}.\nabla\mathbf{u}) = -\nabla p + \mu\nabla^2\mathbf{u} + \rho_e\mathbf{E} \tag{23}$$

where ρ is fluid density, μ is dynamic viscosity, $\mathbf{u}$ is velocity, and p is pressure. This equation is solved in 2 dimensions, along with the continuity equation,

$$\nabla.\mathbf{u} = 0 \tag{24}$$

The resulting simulation provides a solution for ionic wind. Both an electromagnetic and a fluid flow simulation are run concurrently. To achieve this, the variables that are tested need to be used to calculate the values used in the simulation. This is quite a

challenging task, as the lack of validation and testing means that several variables that depend on the specific geometry have to be estimated. This is a major hurdle to gaining an accurate simulation, as the values for these variables have to be based on data obtained from similar testing carried out by Strzelczyk and Gałek [27]. The mathematical model suggested and validated by Gałek and Strzelczyk [27] is based on a point discharge and is as follows:

$$I = KV(V - V_0) \tag{25}$$

where I is the current discharge, V is the supply voltage, V_0 is the supply voltage at the corona onset, and K is a constant defined by the geometry and ion mobility of the ion generator. K can, however, be estimated with the following equation:

$$K = AdB \tag{26}$$

where d is the length between electrodes, and A and B are both constants depending on the geometry of the test area. For these simulations, values of 482 and -3.15 were used for A and B, respectively, to bring them in line with results obtained by Strzelczyk and Gałek [27]. Finally, the equation defining the speed of the discharge air follows the equation

$$u = \mu k \tag{27}$$

where μ is the ion mobility, and k is the constant dependent on geometry. To bring values in line with previous work [28], a value of 0.00786 was chosen for the value of k. So, for 10 mm spacings with 15 kV between them, the value of u could be found to be 34.7 m/s of discharge velocity. The voltage difference between the two electrodes was set as initially as 15 kV and varied up to 40 kV.

The domain used is two-dimensional and is a rectangular box of dimensions 40 mm $\times$ 250 mm. Standard atmospheric conditions were used. The emitter electrode was assumed to be a 0.025 mm circular cross-section, whereas a 2.5 mm circular cross-section diameter wire was used for the collector electrode. This equates to ionization regions for the emitter and collector of 0.16 mm and 1.6 mm, respectively. These values were used as circular boundary conditions, with velocity inlet being normal to the boundary of +34.7 m/s for the emitter and 6 m/s for the collector. Spacing of various lengths was applied between the two electrodes between 10 mm and 50 mm.

The boundary conditions at the outer boundaries of the fluid domain were set as electrically insulated to represent acrylic walls, with the upper and lower boundaries set as no-slip walls, and the left (inlet) and right (outlet) boundaries set as zero pressure to enable outflow in either direction, as can be seen Figure 2a.

The mesh generation was targeted to allow for detail around the two electrodes, with less detail being produced around the outer walls. To achieve this, a two-dimensional automated polygon mesh was used with an additional 10 prism layers to add detail around the ionization region. A mesh convergence study was performed from a base size of 4 mm to 0.0005 mm. The convergence study was performed using the total momentum in the x-direction.

The total momentum quickly converges once the base size has reached a value of 0.015 m and continues at that value without much deviation past a base size value of 0.001. Overall, a base size of 0.001 m was chosen, as it had enough detail around the circumference of the small electrode that the program allowed for the addition of prism layers around it, of which there were 10 added with a total thickness of 0.00005 m so that there would be a smooth transition between the base mesh and the prism layers. Also, the target growth rate was chosen to be 1.1 so that the mesh size did not expand too quickly and lose detail in the

area between the two electrodes, a factor which is most important. The final mesh can be seen in Figure 2b,c.

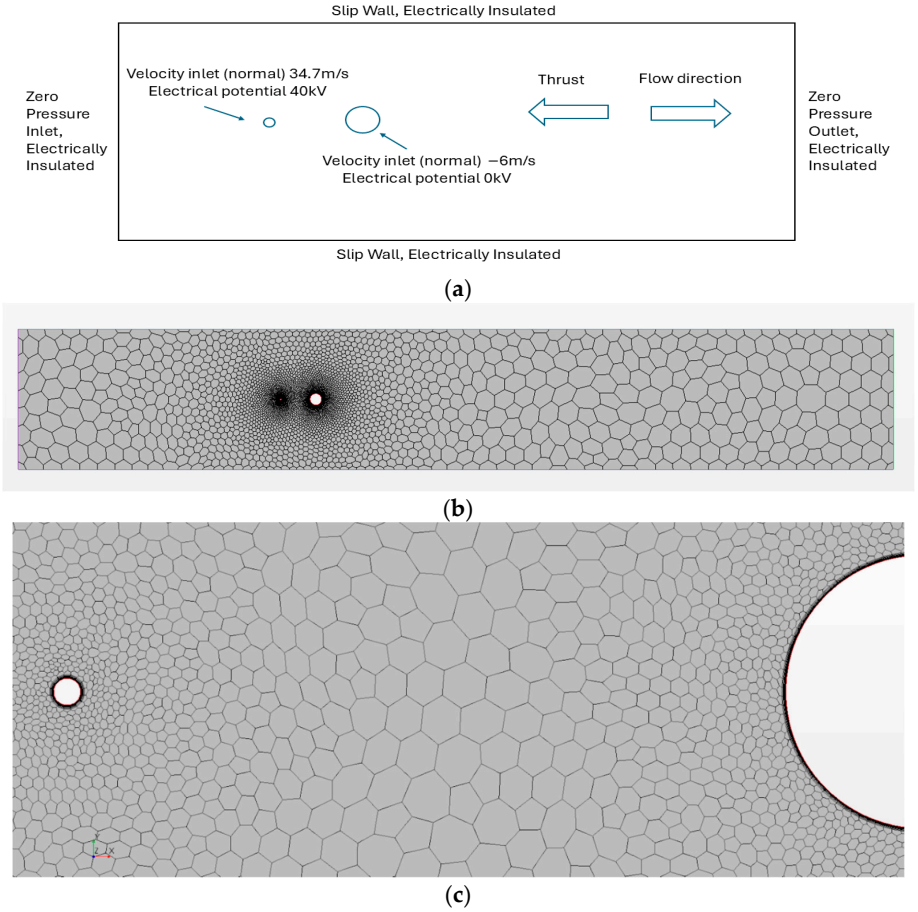

Figure 2. Simulation of (**a**) boundary conditions (not to scale), (**b**) mesh of whole domain, and (**c**) zoomed-in section between electrodes.

Further evaluation of mesh metrics such as skewness angle and face validity aids in identifying if there are any regions of poor resolution or distortion. The simulation is run as a steady-state solution. The model uses a segregated solver for its stability and versatility when solving steady-state simulations. Due to the low Reynolds number, the laminar model was chosen, and the density of the air was constant as 1.226 kg/m^3. Because the modelling of the electromagnetic environment is an important part of the simulation, the optional electromagnetic module was added using electrohydrodynamic potential to model the passage of electric fields through the fluid.

The theoretical calculation described in the previous section is aimed at deriving the thrust in one direction along the horizontal axis. The velocities calculated from the numerical solution are in 2 dimensions; however the forces cancel in the vertical direction due to symmetry, and so only forces in the horizontal plane are considered.

5. Results

5.1. Theoretical Calculations at 15 kV

Theoretical results are collected using the formulae listed in Section 3. We chose 15 kV as an arbitrary voltage to test. The critical distance where the corona discharge becomes a spark and breaks down in the air was calculated to be approximately 7.5 mm. Hence, the theoretical calculations start with 10 mm electrode spacing and increase by increments of 5 mm up to 50 mm. Ionic wind speed can be seen in Figure 3a to be inversely proportional

to the distance between electrodes. As electrode spacing increases, the ionic wind speed decreases. This trend is also true for the thrust and average electric field, as can be seen in Figure 3b.

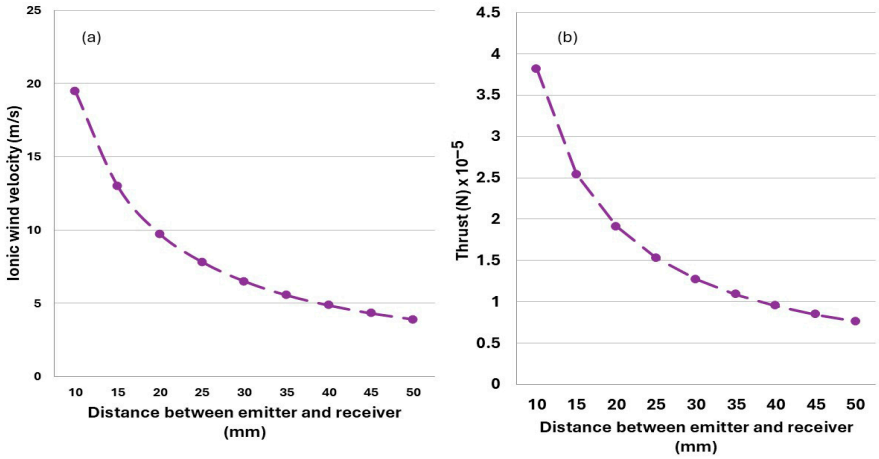

Figure 3. Variation in (**a**) ionic wind velocity and (**b**) theoretical thrust with various electrode spacings.

The maximum theoretical ionic wind velocity achieved is 19.455 m/s at 10 mm spacing with 15 kV. The thrust generated vs. electrode spacing follows the same trend as the ionic wind velocity. Ion engines generally do not produce much thrust, a notion which is supported by previous experiments and analytical calculations in the literature review. The theoretical thrust produced is incredibly small. The maximum thrust achieved using 15 kV at 10 mm electrode spacing is 3.81×10^{-5} Newtons.

5.2. Electromagnetism Modelling Results

From the conditions set up above, the simulation results were calculated, and these results can be seen below. Electromagnetic simulations like the ones shown in Figure 4a–c allow us to see how factors such as electrode distance and voltage difference change the average electrical field strength.

The electromagnetic simulation results show that the electromagnetic field was highly dependent on the change in the gap length. The average electric field strength decreases when the two electrodes are pulled apart. The average electric field strength was measured at the faces of the two electrodes using an inbuilt report in star CCM+. Testing simulation results also suggest that there is a strong relationship between the difference in voltage and the average electric field strength. These relationships are important because they define the base on which the velocity for simulations on wind velocity were based.

5.3. Flow Modelling Results

Following on from electromagnetic modelling, the flow modelling results are similarly affected by both distance between electrodes and voltage difference, as well as the electric field on which the flow model is placed on top of. The results of the flow modelling can be seen in Figure 5a–c. The output velocity was taken as an average across the face of the outlet of the bounding box. The output velocity for varying voltages and spacings is shown in Figures 6 and 7, respectively.

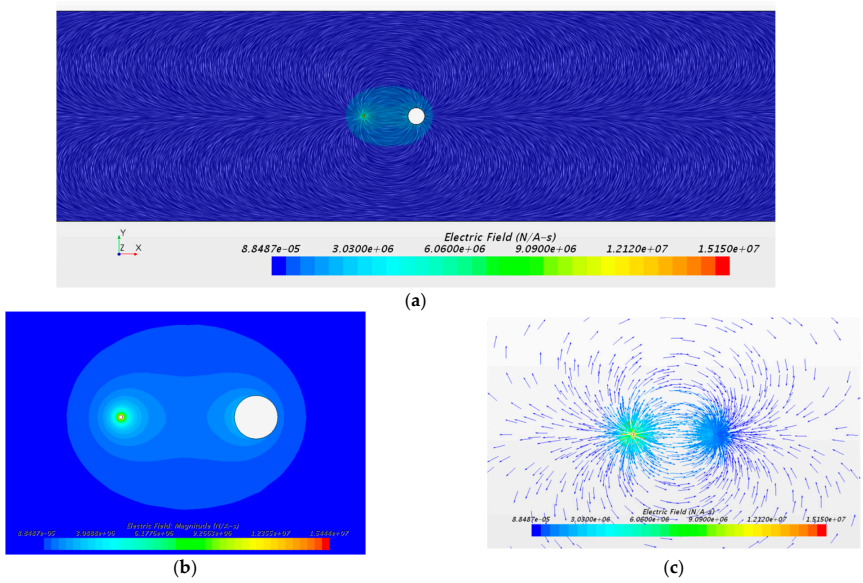

(**a**)

(**b**) (**c**)

Figure 4. Electric field between electrodes (**a**) zoomed out and (**b**) zoomed in with the electric field strength, and (**c**) direction of the electrical field lines.

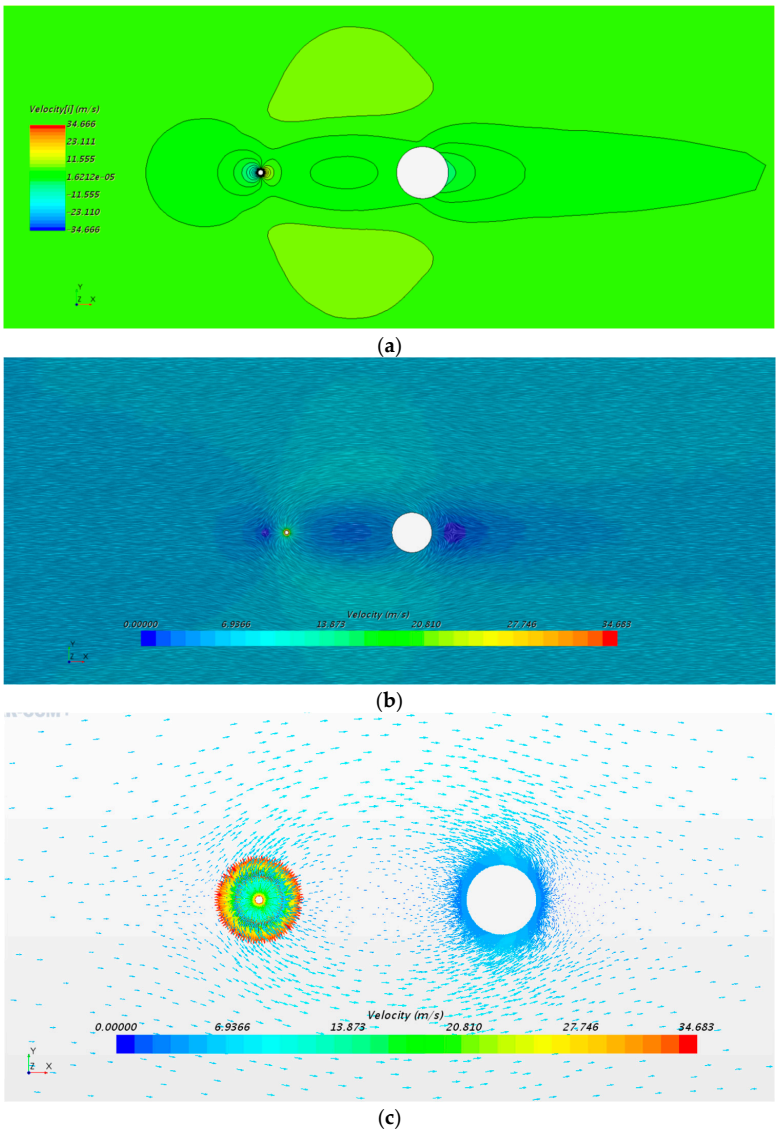

(**a**)

(**b**)

(**c**)

Figure 5. Velocity of air between electrodes: (**a**) scalar, (**b**) generalized flow, and (**c**) vector field.

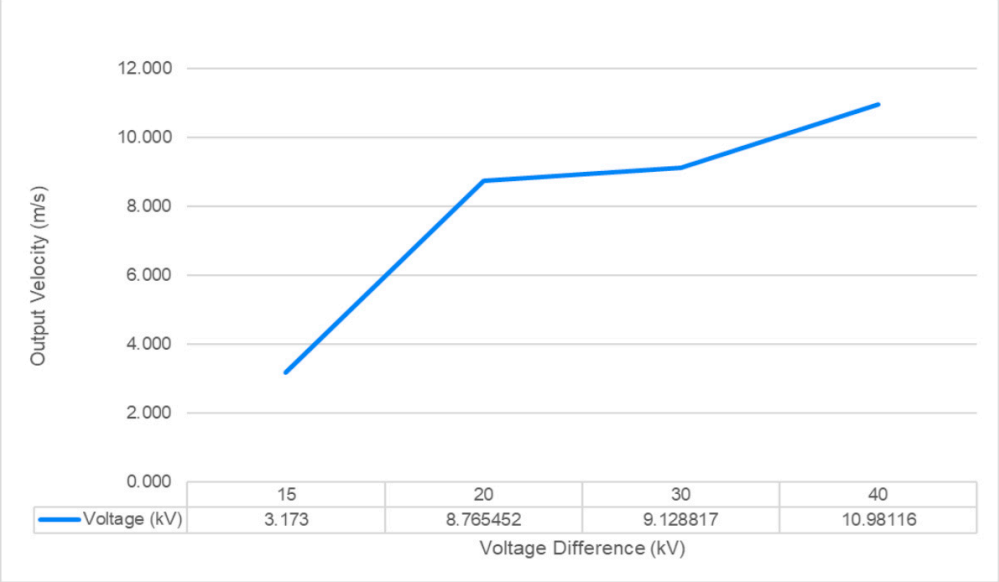

Figure 6. Plot showing the link between output velocity and voltage between the electrodes at 10 mm spacing between electrodes.

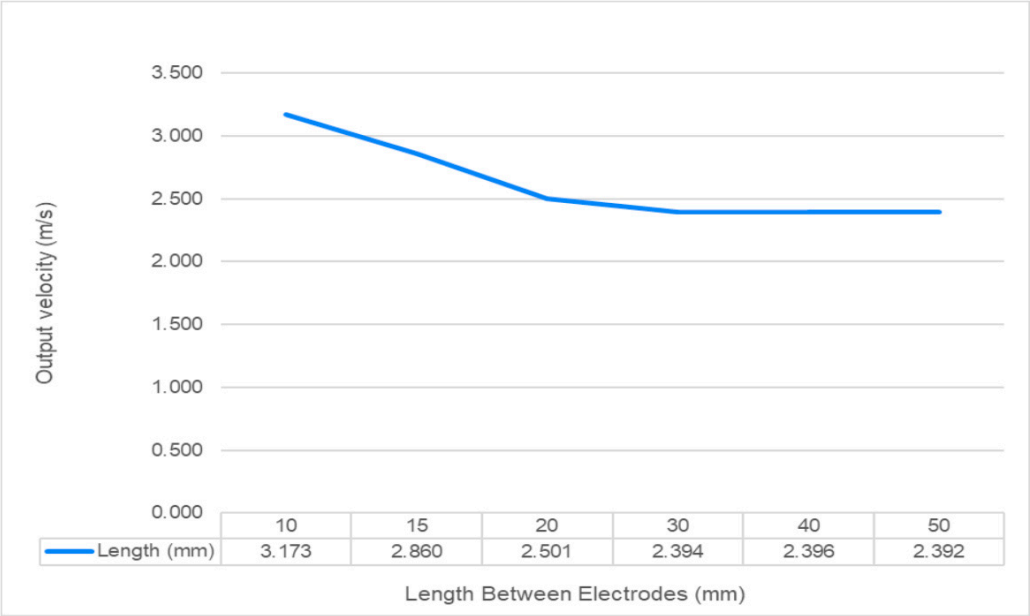

Figure 7. Plot showing the link between output velocity and spacing between the electrodes at a voltage of 15 kV.

As can be seen from the figures above, there is a clear link between output velocity and both voltage difference and the spacing between electrodes. With higher voltage, the velocity of the ionic wind increases. The velocity decreases initially with higher spacings and then appears to be near constant at spacings greater than 30 mm. Figure 8 shows a comparison between numerical and theoretical estimates of ionic wind with varying spacings between electrodes.

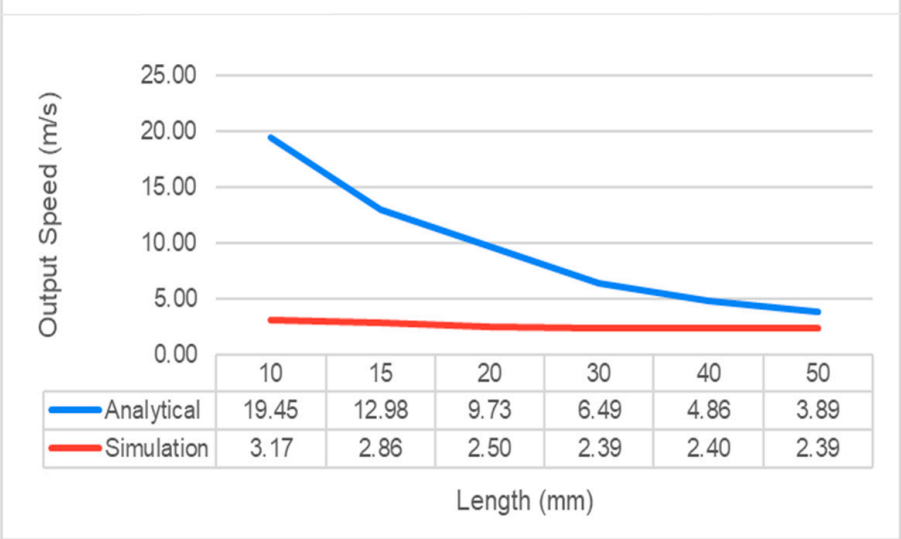

	10	15	20	30	40	50
Analytical	19.45	12.98	9.73	6.49	4.86	3.89
Simulation	3.17	2.86	2.50	2.39	2.40	2.39

Figure 8. Plots showing a comparison between the analytical and simulation results at 15 kV.

Figure 8 shows the same trend between the analytical and simulation results, but a significant difference in terms of the magnitudes. Clearly, the simulation work underestimates the speed with respect to the analytical predictions. Further work is required to fully address these differences and to refine the simulation and analytical models. In particular, the system is dependent on temperature and humidity effects, which have not been considered here.

6. Conclusions

In conclusion, the theoretical ionic wind velocity was estimated to have different voltages and spacings. The relationship between voltage, electrode distance, thrust, and wind speed was reported. A method using CFD simulations attempting to model the natural phenomenon known as ionic wind was shown to predict similar trends to theory; in particular, the ionic wind velocity was found to increase with the voltage over the range considered from 15 kV to 40 kV and to decrease with the separation of the electrodes. The flow field between and around the electrodes was also presented.

The values in this preliminary work are underestimated when compared to theoretical predictions. Further work to enhance the modelling of the interaction between electrodes is predicted to improve the findings. This includes the geometrical configuration and sensitivities due to changes in temperature and humidity. Further analysis of the theoretical formulations and assumptions used are also envisaged to improve the correlation, including any configuration dependency. Nevertheless, the preliminary results and theoretical predictions presented herein provide a framework to improve the numerical modeling of ionic propulsion.

Author Contributions: Conceptualization, J.K. and M.G.; methodology, J.K., M.G., E.K., B.H., E.J.T., N.L.V.M. and D.G.C.; software, B.H., E.J.T., N.L.V.M. and D.G.C.; validation, B.H., E.J.T., N.L.V.M. and D.G.C.; formal analysis, J.K., M.G., B.H., E.J.T., N.L.V.M., D.G.C., J.B., E.K. and A.L.; investigation, B.H., E.J.T., N.L.V.M. and D.G.C.; data curation, B.H., E.J.T., N.L.V.M. and D.G.C.; writing—original draft preparation, B.H., E.J.T., N.L.V.M., and D.G.C.; writing—review and editing, J.K., M.G., J.B., E.K. and A.L.; supervision, J.K. and M.G.; project administration, J.K. and M.G. All authors have read and agreed to the published version of the manuscript.

Funding: This research received no external funding.

Data Availability Statement: The original contributions presented in this study are included in the article. Further inquiries can be directed to the corresponding author.

Acknowledgments: The authors would like to acknowledge previous work by Arundeep Matharu, Nikesh Mehta, Ziaul Hoque, Carlson Ddamba, and David Bickersteth on which the current work is based.

Conflicts of Interest: Author Bradley Horne was employed by the company Veolia. Edward Taylor was employed by the company Renishaw. Ethan Krauss is the director of the company Electron Air LLC. The remaining authors declare that the research was conducted in the absence of any commercial or financial relationships that could be construed as a potential conflict of interest.

References

1. Guericke, O. Von Experimenta Nova (ut Vocantur) Magdeburgica de Vacuo Spatio 1672. Available online: https://archive.org/details/experimentanovau00gueruoft (accessed on 25 September 2025).
2. Brewster, D.; Kane, R.; Francis, W. *The London, Edinburgh and Dublin Philosophical Magazine and Journal of Science*; Taylor & Francis: London, UK, 1864; p. 214. Available online: https://play.google.com/store/books/details?id=EptJAAAAYAAJ&rdid=book-EptJAAAAYAAJ&rdot=1 (accessed on 15 September 2025).
3. Schatzkin, P. *The Man Who Mastered Gravity: A Twisted Tale of Space, Time and the Mysteries In Between*; Incorrigible Arts: Nashville, TN, USA, 2023.
4. Krauss, E.D. Self Contained Ion Powered Aircraft. U.S. Patent US10119527B2, 6 November 2018.
5. Chu, J. MIT engineers fly first-ever plane with no moving parts. *MIT News* 2018. Available online: https://news.mit.edu/2018/first-ionic-wind-plane-no-moving-parts-1121 (accessed on 25 September 2025).
6. Khomich, V.Y.; Rebrov, I.E. In-atmosphere electrohydrodynamic propulsion aircraft with wireless supply onboard. *J. Electrostat.* **2018**, *95*, 1–12. [CrossRef]
7. Grosse, S.; Benard, N.; Moreau, E. Electroaerodynamic thrusters: Influence of a freestream on the current, ionic wind, and force produced by a DC corona discharge. *J. Electrost.* **2024**, *130*, 103950. [CrossRef]
8. Xu, H.; Gomez-Vega, N.; Agrawal, D.R.; Barrett, S.R. Higher thrust-to-power with large electrode gap spacing electroaerodynamic devices for aircraft propulsion. *J. Phys. D Appl. Phys.* **2020**, *53*, 025202. [CrossRef]
9. Xu, H.; He, Y.; Strobel, K.L.; Gilmore, C.K.; Kelley, S.P.; Hennick, C.C.; Barrett, S.R. Flight of an aeroplane with solid-state propulsion. *Nature* **2018**, *563*, 532–535. [CrossRef] [PubMed]
10. Electron Air LLC Homepage. Available online: https://electronairllc.org/ (accessed on 25 September 2025).
11. Krauss, E.D. Ion Propelled Vehicle. U.S. Patent US11161631B2, 2 November 2021.
12. He, Y.; Perreault, D.J. Lightweight High-Voltage Power Converters for Electroaerodynamic Propulsion. *IEEE J. Emerg. Sel. Top. Ind. Electron.* **2021**, *2*, 453–463. [CrossRef]
13. Allen, P.H.G.; Karayiannis, T.G. Electrohydrodynamic enhancement of heat transfer and fluid flow. *Heat Recover. Syst. CHP* **1995**, *15*, 389–423. [CrossRef]
14. Jewell-Larsen, N.E.; Ran, H.; Zhang, Y.; Schwiebert, M.K.; Tessera, K.A.H.; Mamishev, A.V. Electrohydrodynamic (EHD) cooled laptop. In Proceedings of the 25th Annual IEEE Semiconductor Thermal Measurement and Management Symposium, San Jose, CA, USA, 15–19 March 2009; pp. 261–266. [CrossRef]
15. Locke, B.R.; Sato, M.; Sunka, P.; Hoffmann, M.R.; Chang, J.S. Electrohydraulic discharge and nonthermal plasma for water treatment. *Ind. Eng. Chem. Res.* **2006**, *45*, 882–905. [CrossRef]
16. Bouazza, M.R.; Yanallah, K.; Pontiga, F.; Chen, J.H. A simplified formulation of wire-plate corona discharge in air: Application to the ion wind simulation. *J. Electrostat.* **2018**, *92*, 54–65. [CrossRef]
17. Chirita, M.; Ieta, A. Toroidal counter electrode for ionic propulsion. *Sci. Rep.* **2022**, *12*, 19002. [CrossRef] [PubMed]
18. Hogg, M.G.; Timoshkin, I.V.; Macgregor, S.J.; Wilson, M.P.; Given, M.J.; Wang, T. Electrical breakdown of short non-uniform air gaps. In Proceedings of the IEEE International Pulsed Power Conference, San Francisco, CA, USA, 16–20 June 2013; pp. 5–8. [CrossRef]
19. Wan, Y.; Zhang, X.; Li, J. Electromagnetic Environment of UHVDC System. In *Ultra-High Voltage AC/DC Power Transmission*; Springer: Berlin/Heidelberg, Germany, 2017; pp. 1059–1106.
20. Yan, P.; Zheng, C.; Zhu, W.; Xu, X.; Gao, X.; Luo, Z.; Cen, K. An experimental study on the effects of temperature and pressure on negative corona discharge in high-temperature ESPs. *Appl. Energy* **2016**, *164*, 28–35. [CrossRef]
21. Chen, S.; Nobelen, J.C.P.Y.; Nijdam, S. The effect of humidity on ionic wind velocity in ambient air. In Proceedings of the 69th Annual Gaseous Electronics Conference (GEC 2016), Bochum, Germany, 10–14 October 2016; p. HT6.00074.

22. Lee, J.R.; Lau, E.V. Effects of relative humidity in the convective heat transfer over flat surface using ionic wind. *Appl. Therm. Eng.* **2017**, *114*, 554–560. [CrossRef]
23. Perkins, H.D.; Thompson, W.K.; An Investigation of Ionic Wind Propulsion. *NASA Tech. Rep*. 2009. Available online: https://ntrs.nasa.gov/api/citations/20100000021/downloads/20100000021.pdf (accessed on 25 September 2025).
24. Christenson, E.A.; Moller, P.S. Ion-Neutral Propulsion in Atmospheric Media. *AIAA J.* **1967**, *5*, 1768–1773. [CrossRef]
25. Sigmond, R.S. Simple approximate treatment of unipolar space-charge-dominated coronas: The Warburg law and the saturation current. *J. Appl. Phys.* **1982**, *53*, 891–898. [CrossRef]
26. Tyndall, A.M.; Grindley, G.C. The mobility of ions in air—Part I. Negative ions in moist air. *Philos. Trans. R. Soc. Lond. A* **1926**, *110*, 341–358.
27. Gałek, R.; Strzelczyk, P. Velocity profiles of an electrohydrodynamic flow generator: CFD and experiment. *J. Electrostat.* **2019**, *99*, 19–30. [CrossRef]
28. Knight, J.; Khan, A.A.; Hossain, M.S.; Fotouhi, M.; Steuwer, A.; Khan, A.; Kurtulus, D.F. CFD Modelling of Ionic Propulsion. In Proceedings of the First International Conference on Aeronautical Sciences, Engineering and Technology (ICASET 2023), Singapore, 14–16 November 2023; Khan, A.A., Hossain, M.S., Fotouhi, M., Steuwer, A., Khan, A., Kurtulus, D.F., Eds.; Springer: Singapore, 2024. [CrossRef]